Real-time Subsea Communication Cable Detection for AUV-based Inspection

Adrian Bodenmann, Ibrahim Fadhil Djauhari, Jivan Devgon and Blair Thornton
University of Southampton
Southampton, UK
adrian.bodenmann@soton.ac.uk

***Abstract*—This paper proposes a method for visual inspection of subsea communication cables. As principal carrier for data transmission between continents and islands, such cables are major infrastructure assets that are vulnerable to natural or human causes of damage, but are challenging to survey due to the long distances they span and great water depths they are laid in. AUVs can visually map seafloor cables; however, autonomous cable following along routes with relatively high uncertainties and over varying substrate types is challenging. This research develops a cable detection and following algorithm for real-time on-board processing on camera-equipped AUVs. Simulations on existing cable routes demonstrate effective and repeatable cable following despite introducing random misdetections at the rates expected for the suggested machine learning based image classifier. A study on various levels of incorrect cable detection and different vehicle speeds shows that a low level of false positives in the cable detection is crucial for robust cable following, and lower vehicle speeds lead to a higher visual coverage of cable routes, albeit at an increased survey time.**

***Index Terms*—subsea cable, monitoring, seafloor mapping, AUV, machine learning, AI, image classification**

I. Introduction

The world has become heavily reliant on global data communication, 97% of which is transmitted via subsea cables [1]. Reliable connections are vital, as the socioeconomic cost of any interruption is high and wide-ranging. Currently, there are over 1.4 million kilometres of subsea communication cables spanning the globe [2]. These cables can get damaged, due to natural causes, such as turbidity currents and earthquakes [3], [4] or unintentional or intentional human activity [5]–[7]. Network redundancy can mitigate interruptions in the event of a cable fault; however, in the event of multiple cable breaks, certain areas can be cut off [6]. This paper proposes visual inspection of subsea communication cables using autonomous underwater vehicles (AUVs) to detect damage or objects that could pose a threat before they cause the cable to break.

Although subsea cables are steel wire armoured and buried in shallow waters, they are unarmoured with a diameter of approximately 3 cm and laid on top of the seafloor at larger depths, which makes it possible to visually inspect the cable with underwater cameras. The images can be used both to detect potential threats as well as navigational features for tracking the cable. While remotely operated vehicles (ROVs) are a versatile tool to inspect underwater infrastructure, their need for a support vessel and crew incurs high costs for routine surveys along cables in deep waters. AUV based camera surveys offer a more economical option to gather the same type of images. However, autonomous cable following is a challenging task for AUVs, as the narrow footprint of the cameras' fields of view requires an AUV to follow cables with minimum (centimetres to metres) lateral offset. Although the estimated positions of subsea cables are recorded during laying, the lateral uncertainty is 5 to 10% of water depth [8], making waypoint-based navigation not precise enough to follow cable routes. This makes real-time cable detection necessary. Electromagnetic sensing is one option to achieve this [9], however, it requires additional sensors on the AUV. Side-scan sonar (SSS) captures the seafloor in relatively high resolution, however, subsea communication cables are in general too thin to be reliably detected in SSS data [10], making it not a viable option for cable tracking. Optical images on the other hand offer high enough resolution to detect cables on the seafloor and cameras are typically already installed on AUVs or can be retrofitted using a range of off-the-shelf solutions.

This research develops and simulates a subsea cable tracking method using an AI-based real-time cable detection algorithm. Imagery from a grid photo survey of the Regional Cabled Array of the Ocean Observatories Initiative at the Southern Hydrate Ridge off the coast of Oregon, USA, was used to train image classification algorithms, and to estimate the accuracies (in particular true and false positives) of these algorithms so that the impact of imperfect detection on cable tracking can be understood. The mapping data also provided examples of real-world cable routes for the simulation. A cable following algorithm was developed and tested with a simulation using the physics model of a Sparus II AUV [11], and using realistic performance of cable identification in images.

II. Method

A. Survey strategy

An AUV is tasked to visually map a subsea communication cable. It is assumed that there is a prior map of where the cable is laid, but lateral uncertainties of up to 10% of depth, which is representative of realworld cable route knowledge. The AUV is deployed in the vicinity where the cable is known to be laid. When the AUV reaches the seafloor, it moves into the

This project is funded by the Defence and Security Accelerator (DASA). Data used for method development was gathered during the FK180731 cruise of the Schmidt Ocean Institute's *R/V Falkor* using the University of Tokyo AUV AE2000F.

direction where the prior map indicates the cable is. When the cable detection algorithm described in section II-B reports detection of the cable, the cable tracking algorithm described in section II-C generates the high-level navigation commands for the AUV to follow the cable. If the cable is not detected, a graph-based Simultaneous Localisation and Mapping (SLAM) method is used to update the search space based on which the navigation commands are determined until the cable is again observed in a camera image [8].

B. Image classification algorithm

The cable tracking algorithm assumes that the AUV acquires strobed images of the seafloor from roughly constant altitude at regular time intervals. The images are colour corrected according to the acquisition altitude using the method described in [12] based on pre-trained colour attenuation parameters. Subsequently they are corrected for lens distortion and stretched or shrunk to normalise the physical dimension a pixel represents to the same size in each image and so compensate for differences in acquisition altitudes due to imperfect terrain following. The images are then split into a grid of square image tiles with associated geolocation information, which are classified using a semi-supervised deep-learning classification algorithm. Two different algorithms for training convolutional neural networks were tested; the location guided autoencoder (LGA) algorithm described in [13], and the GeoCLR algorithm described in [14]. These algorithms were chosen because they are well suited to imagery where objects cover larger areas than what fits into a single image frame, leveraging image location information, and because they have been shown to achieve good classification accuracies for underwater images. In both cases the algorithm uses a model that is pre-trained on a labelled set of images acquired in similar conditions. Training these models is computationally intensive, but can be done offline on a high-specification workstation or on a high-performance PC. Classifying images is a less computationally intense process and can be performed by CPUs typically used on board AUVs.

C. Cable following algorithm

In images where the cable is detected in at least two image tiles, the navigation command for the AUV is computed based on these. The centroid of all image tiles where cable was detected is computed, as well as a regression line across the cable-labelled tiles. A waypoint is generated on the regression line at a distance d from the detected centroid, as shown in Fig. 1. The positive along-the-cable direction from the prior knowledge map is used to determine the side of the detected centroid where the new waypoint needs to be set. This replaces any existing waypoint, and will itself be updated at the next timestep.

Fig. 2 illustrates how the number of tiles into which images are split determines the resolution at which the cable

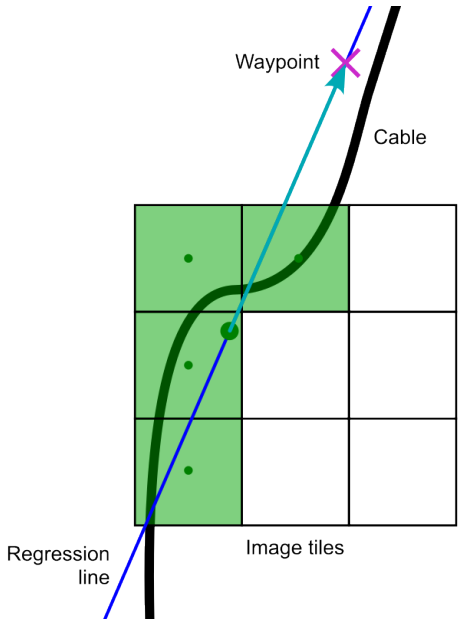

Fig. 1: Illustration of waypoint generation from a seafloor image sampled into 3×3 tiles.

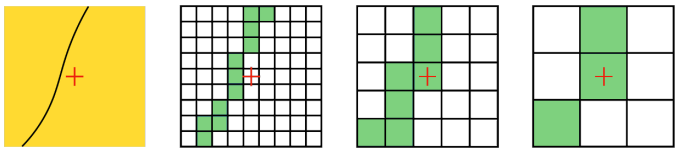

Fig. 2: Illustration of discretising the image footprint, where the red cross is the centre of the image. This also corresponds to the intersection of the camera centre-line with the seafloor.

regression can be computed. For an image footprint of 2×2 m, the computed centroid and bearing of the cable in Fig. 2 are:

$$\begin{aligned}\mathbf{p}_{cable} = \begin{bmatrix} x_o \\ y_o \\ \alpha_o \end{bmatrix} &= \begin{bmatrix} 0 \\ -0.22 \\ 26 \end{bmatrix}_{true} \\ &\approx \begin{bmatrix} 0.02 \\ -0.30 \\ 25.1 \end{bmatrix}_{9\times9} \approx \begin{bmatrix} -0.16 \\ -0.40 \\ 31.6 \end{bmatrix}_{5\times5} \approx \begin{bmatrix} 0.0 \\ -0.22 \\ 33.7 \end{bmatrix}_{3\times3}.\end{aligned} \tag{1}$$

Grids with a larger number of tiles lead to a better resolution of the cable modelling. However, this also increases the computational load for classification and reduces its labelling accuracy. Errors due to incorrect cable detections can cause unbounded errors in the cable route modelling through false positive detections. Although grids with fewer tiles lead to a lower resolution of the cable modelling, the errors are bounded. Therefore we select a small number of larger grid elements to maximise detection accuracy.

D. Simulator

A simulation was implemented to test the algorithm and to determine its performance in terms of proportion of cable observed and time taken under different conditions for a given

Fig. 3: The "Smarty200" Iqua Sparus II AUV owned and operated by the University of Southampton. The AUV is modified to integrate a high-resolution seafloor imaging system and a Doppler aided inertial navigation system.

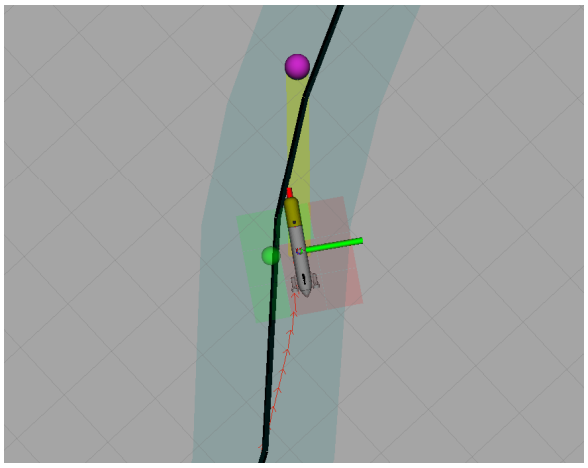

Fig. 4: Simulator showing the Sparus II AUV imaging the cable (black), where green indicates presence and red absence of cable in the respective image tiles, and purple the current waypoint.

cable route. We assume that the survey is carried out with an Iqua Sparus II AUV, pictured in Fig. 3. The simulation is based on the Robot Operating System (ROS) and uses the vehicle dynamics model provided by the AUV manufacturer. A module for modelling cable routes and tiled image acquisition and classification thereof was implemented, as shown in Fig. 4. Errors in image classification can be modelled by indicating the ratio of false negatives (cable not detected where cable is present) and false positives (image tile flagged as containing cable even though there is no cable in the respective image tile). The recordings of simulated camera poses and the model of its field of view are used to compute the percentage of observed cable for each run, as illustrated in Fig. 5.

III. Results

A. Image classification

The LGA and GeoCLR algorithms were trained on a grid mapping dataset of the Ocean Observatory Initiative Regional Cabled Array at the Southern Hydrate Ridge off the coast of Oregon, USA. The data was collected from an altitude of 6 m above the seafloor with the SeaXerocks3 visual mapping device mounted on the AE2000f AUV of the University of

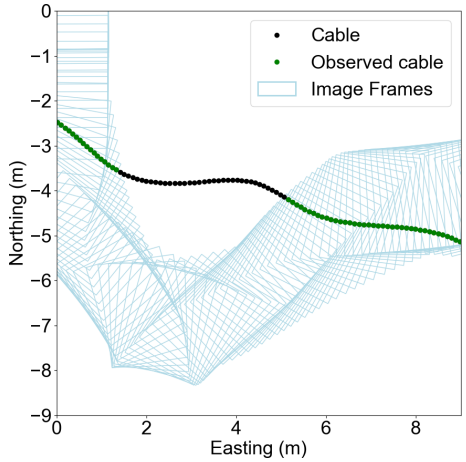

Fig. 5: Visualisation of the camera frames for each observation in a cable tracking simulation run, assuming a 46° × 60° camera field of view and a mapping altitude of 2 m over a flat seafloor.

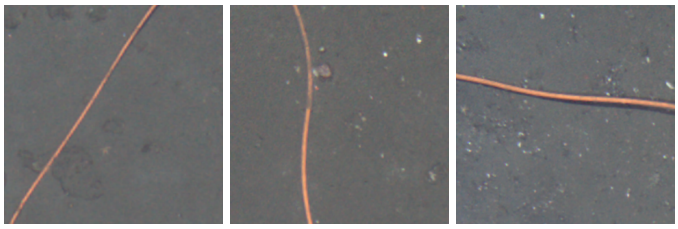

Fig. 6: Examples of image tiles showing the subsea communication cable.

Tokyo, deployed from *R/V Falkor* of the Schmidt Ocean Institute [15]. The colour correction parameters were determined using all images of the dataset and applied back on the images. After correcting for lens distortions, the images were split into tiles corresponding to 1.6 m by 1.6 m squares of seafloor at 5 mm per pixel resolution, leading to 3x3 tiles per image for most images. The tiles were divided into categories "cable", "rock", "carbonate", "sand", "shell fragment" and "bacterial mat" based on manual labelling data. Fig. 6 shows examples of image tiles picturing the cable. While for cable following distinguishing beyond "cable" and "not cable" is not required, using the additional classes of different types of substrates provides further information for analysis, including where false detections are more likely to occur.

CNN models were trained on the images using the self-supervised feature learning LGA and GeoCLR algorithms. Nonlinear support vector machine (SVM) with a radial basis function (RBF) kernel classifiers were trained to delineate class boundaries in the feature space using the labelled data. Fig. 7 shows the t-distributed stochastic neighbour embedding (t-SNE) representation of the feature space of the image tiles. While clear delineation of classes in the dimension-reduced t-SNE representation enables accurate classification in most cases, some degree of mixing does not necessarily lead to bad classification results. The performance of the classifiers

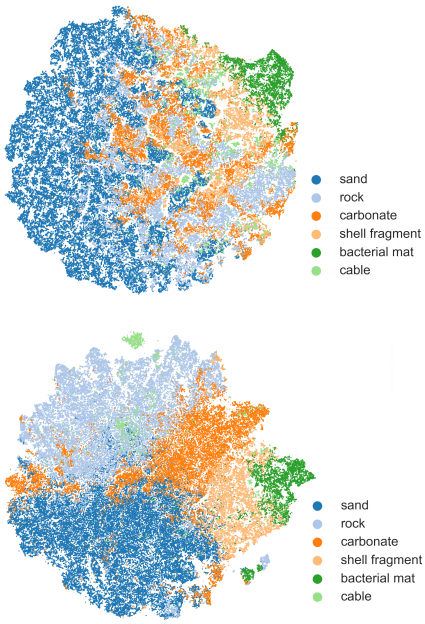

Fig. 7: T-SNE visualisation of the feature space after applying the LGA (top) and GeoCLR (bottom) model on the labelled image tiles.

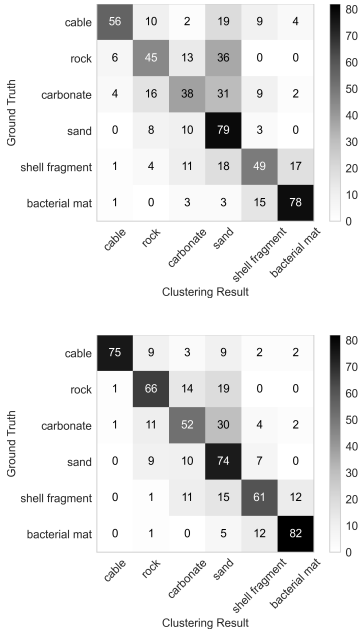

Fig. 8: Confusion matrices between clustering results and ground truth for the LGA (top) and GeoCLR (bottom) classifier using 100 labelled image tiles for each class.

from both models were analysed by applying them on 100 image tiles of each class that had not been used for training of the classifiers. The confusion matrices in Fig. 8 show good performance for both models for cable detection. The precision for the cable class is 0.82 for the LGA classifier and 0.97 for GeoCLR, the recall 0.56 and 0.75, and the F1-score is 0.67 and 0.85, making GeoCLR the better performing classifier by all measures, showing relatively reliable detection capabilities for seafloor cables. The LGA algorithm yielded 44% false negatives and 12% false positives for the cable class, whereas GeoCLR lead to 25% false negatives and 2% false positives. While failure to detect the cable in an image tile (false negative) can lead to a slightly different vector for the waypoint generation, or no image-based waypoint generation, false positives (reporting cable where there is none) can lead to random waypoint generation, leading the AUV off course. For these reasons, while correct detection is important in general, it is crucial that the rate of false positives is low for tracking purposes.

B. Simulation of cable tracking

For the simulation a mapping altitude of 2 m above a flat seafloor with a camera field of view of 46° × 60°, leading to a projected area of 1.7 m × 2.3 m and an image acquisition rate of 1 Hz were assumed to simulate Smarty200's camera system. A 100 m long section of cable route mapped at the Southern Hydrate Ridge was used in the simulation, and the distance d at which a waypoint is set in front of the centre of cable observations was set to 3 m. The performance of cable tracking was determined for different conditions of AUV speeds and cable detection accuracies. The cable detection accuracies from the LGA and GeoCLR application to the Southern Hydrate Ridge data, as well as error-free detection were simulated. While the imagery at Southern Hydrate Ridge had been acquired from higher altitude than the 2 m assumed for the simulation, these levels represent upper bounds, as clearer images acquired from lower altitudes are likely to yield better detection accuracies. Additionally, the influence of vehicle speed was studied using 3 different AUV surge speeds and the expected detection accuracies based on the better performing GeoCLR algorithm. For each setting 10 repeat runs were simulated. Fig. 9 shows the AUV tracks for the 10 runs of each tested condition, and table I shows the average and the standard deviation of the cable coverage and time taken for mapping the cable track. A run was considered completed when passing the last cable point in the along-the-cable direction as per the prior cable map.

As expected, the highest cable observation rate was achieved with simulated error-free cable detection, plotted in Fig. 9a. The false positive detection rates of 12% as found when applying the LGA algorithm to the Southern Hydrate Ridge dataset caused the AUV to lose track of the cable where it bends, with the SLAM algorithm unable to guide the AUV back towards the cable within the short survey distance, as Fig. 9b and Fig. 9d show, leading to a cable observation rate of only 11.2% ± 3.8% (with no false negatives) and 12.6% ± 3.4% (with false negatives) for the studied cable route at the AUV's default surge speed of 0.2 m/s.

The comparison between simulated cable detection with only false positives (Fig. 9b and 9e) and only false negatives (Fig. 9c and 9f) confirm that false positive cable detections have a stronger detrimental effect on the performance than

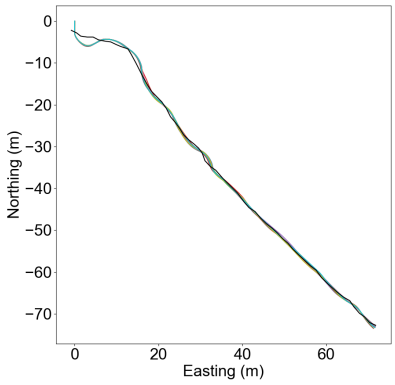

(a) Speed: 0.2 m/s, false positives: 0%, false negatives: 0%

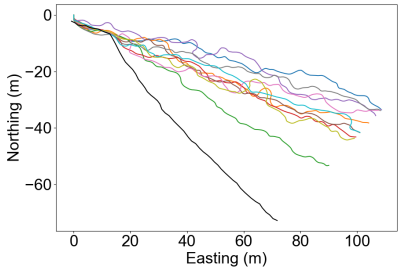

(b) Speed: 0.2 m/s, false positives: 12%, false negatives: 0%

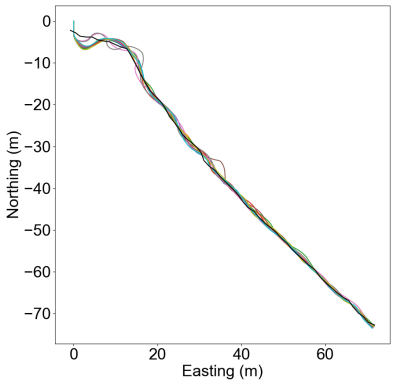

(c) Speed: 0.2 m/s, false positives: 0%, false negatives: 44%

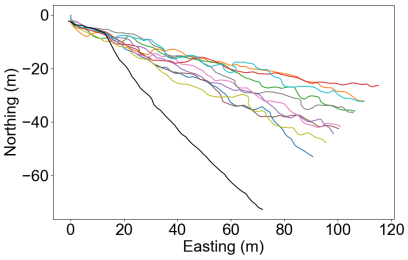

(d) Speed: 0.2 m/s, false positives: 12%, false negatives: 44%

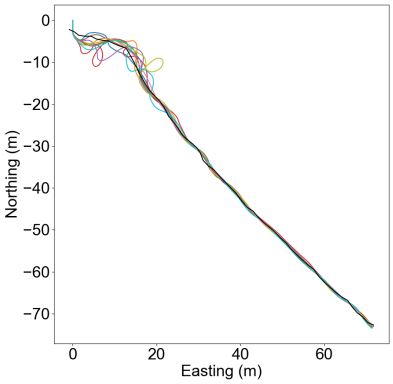

(e) Speed: 0.2 m/s, false positives: 2%, false negatives: 0%

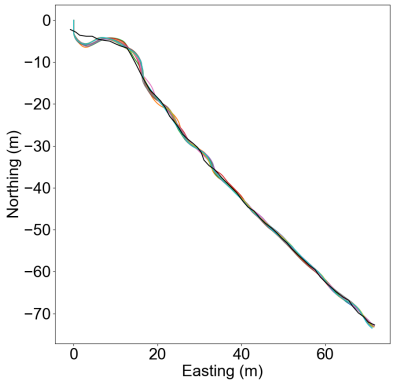

(f) Speed: 0.2 m/s, false positives: 0%, false negatives: 25%

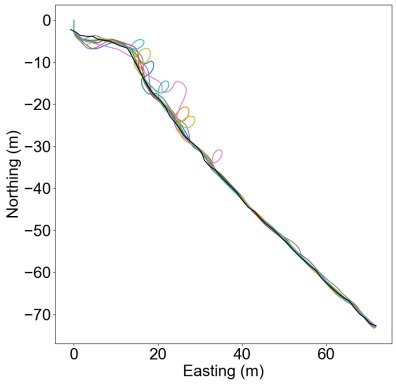

(g) Speed: 0.15 m/s, false positives: 2%, false negatives: 25%

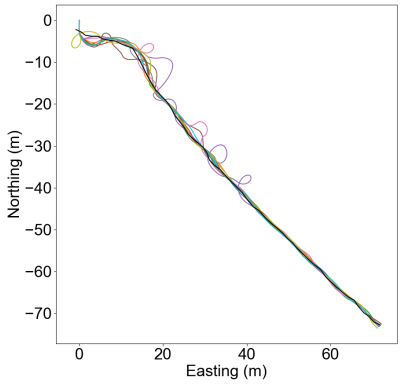

(h) Speed: 0.2 m/s, false positives: 2%, false negatives: 25%

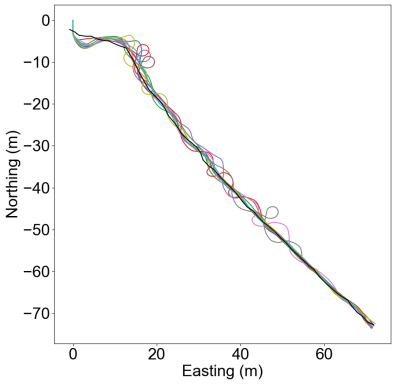

(i) Speed: 0.3 m/s, false positives: 2%, false negatives: 25%

Fig. 9: Cable route (black) and AUV tracks (in colours) from 10 repeat simulation runs for the different tested configurations of false positive and negative cable detection rates and AUV surge speeds.

TABLE I: Average duration and portion of observed cable ($\pm$ std. dev.) for different cable detection accuracy rates and vehicle speeds. The cases for full LGA and GeoCLR detection accuracy rates and typical Smarty200 survey speed (0.2 m/s) are shown in bold.

AUV speed (m/s)	False positives (%)	False negatives (%)	Duration (s)	Observed cable (%)
0.2	0	0	538.2 $\pm$ 0.9	95.4 $\pm$ 0.8
0.2	12	0	590.0 $\pm$ 27.3	11.2 $\pm$ 3.8
0.2	0	44	544.8 $\pm$ 6.1	91.9 $\pm$ 3.0
0.2	**12**	**44**	**583.4 $\pm$ 25.4**	**12.6 $\pm$ 3.4**
0.2	2	0	558.4 $\pm$ 29.0	90.1 $\pm$ 3.5
0.2	0	25	539.7 $\pm$ 2.9	93.1 $\pm$ 2.6
0.15	2	25	754.8 $\pm$ 49.2	93.0 $\pm$ 6.8
0.2	**2**	**25**	**563.8 $\pm$ 44.3**	**90.3 $\pm$ 4.7**
0.25	2	25	465.3 $\pm$ 23.7	79.1 $\pm$ 8.1

false negatives, even if the false negatives occur at a higher rate. With a false positive detection rate of 2% and false negative rate of 25% found when applying the GeoCLR algorithm on the Southern Hydrate Ridge data, the simulation in Fig. 9h shows good cable following performance and a 90.3% $\pm$ 4.7% cable observation rate for the studied cable route. False detections still occasionally lead the AUV away from the cable route, but the SLAM algorithm succeeded in guiding it back without the false detections excessively deteriorating the SLAM solution. The simulations of different AUV surge speeds and false cable detection rates based on the GeoCLR performance plotted in Fig. 9g to 9i show that slower surge speeds lead to better observation rates, although it increases the required time for the survey.

IV. Conclusions and future work

This paper proposes a method for tracking subsea communication cables using camera images. Results from 2 different algorithms applied to a set of subsea communication cable images acquired by an AUV show good detection performance, where the GeoCLR algorithm outperforms LGA. A simulation implementing the proposed cable tracking algorithm applied to an existing cable route demonstrates the importance of accurate cable detection, where the simulation using false detection rates typical for GeoCLR lead to good cable mapping rates and so confirms the validity of the algorithm, while the lower correct cable detection rates typical of the LGA algorithm were shown not to be sufficient for reliable cable following.

The algorithm will be implemented on the Smarty200 AUV of the University of Southampton and tested at sea on a stretch of temporarily laid subsea communication cable to prove the method and assess the real-time performance in a relevant environment. Further studies will look into the effects of partially buried cable sections and will be extended to other cable routes.

References

[1] R. Sunak, "Undersea cables - Indispensable, insecure," 2017. [Online]. Available: https://policyexchange.org.uk/publication/undersea-cables-indispensable-insecure/

[2] "Submarine cable frequently asked questions." [Online]. Available: https://www.telegeography.com/submarine-cable-faqs-frequently-asked-questions

[3] B. C. Heezen and W. M. Ewing, "Turbidity currents and submarine slumps, and the 1929 Grand Banks [Newfoundland] earthquake," *American Journal of Science*, vol. 250, pp. 849–873, Dec. 1952. [Online]. Available: https://ajsonline.org/article/58374

[4] S.-K. Hsu, J. Kuo, C.-L. Lo, C.-H. Tsai, W.-B. Doo, C.-Y. Ku, and J.-C. Sibuet, "Turbidity currents, submarine landslides and the 2006 Pingtung Earthquake off SW Taiwan," *Terrestrial, Atmospheric and Oceanic Sciences*, vol. 19, p. 767, 2008. [Online]. Available: http://tao.cgu.org.tw/index.php/articles/archive/geophysics/item/808

[5] J. Kirk, "Sabotage suspected in Egypt submarine cable cut," *IDG News Service*, 2013. [Online]. Available: https://www.infoworld.com/article/2613497/sabotage-suspected-in-egypt-submarine-cable-cut.html

[6] "Damaged cable leaves Shetland cut off from mainland," *BBC News*, Oct. 2022. [Online]. Available: https://www.bbc.co.uk/news/uk-scotland-north-east-orkney-shetland-63326102

[7] J. Gambrell, "3 Red Sea data cables cut as Houthis launch more attacks in the vital waterway," *Associated Press*, 2024. [Online]. Available: https://apnews.com/article/red-sea-undersea-cables-yemen-houthi-rebels-attacks-b53051f61a41bd6b357860bbf0b0860a

[8] B. Thornton, A. Bodenmann, M. Massot-Campos, S. Simmons, S. Gourvenec, D. White, T. Bennets, and D. Newborough, "Autonomous robotic monitoring of subsea communication cables," in *Underwater Defence Technology 2024*, London, UK, Apr. 2024.

[9] A. V. Inzartsev and A. M. Pavin, "AUV cable tracking system based on electromagnetic and video data," in *OCEANS 2008 - MTS/IEEE Kobe Techno-Ocean*, Kobe, Japan, 2008, pp. 1–6. [Online]. Available: https://ieeexplore.ieee.org/document/4531082

[10] I. Kogan, C. K. Paull, L. A. Kuhnz, E. J. Burton, S. Von Thun, H. Gary Greene, and J. P. Barry, "ATOC/Pioneer Seamount cable after 8 years on the seafloor: Observations, environmental impact," *Continental Shelf Research*, vol. 26, no. 6, pp. 771–787, 2006. [Online]. Available: https://www.sciencedirect.com/science/article/pii/S0278434306000355

[11] M. Carreras, J. D. Hernández, E. Vidal, N. Palomeras, D. Ribas, and P. Ridao, "Sparus II AUV – A hovering vehicle for seabed inspection," *IEEE Journal of Oceanic Engineering*, vol. 43, no. 2, pp. 344–355, 2018.

[12] M. Massot-Campos, T. Yamada, and B. Thornton, "Towards sensor agnostic artificial intelligence for underwater imagery," in *2023 IEEE Underwater Technology (UT)*. IEEE, Mar. 2023, pp. 1–6. [Online]. Available: https://ieeexplore.ieee.org/document/10103403/

[13] T. Yamada, A. Prügel-Bennett, and B. Thornton, "Learning features from georeferenced seafloor imagery with location guided autoencoders," *Journal of Field Robotics*, vol. 38, pp. 52–67, Jan. 2021. [Online]. Available: https://onlinelibrary.wiley.com/doi/10.1002/rob.21961

[14] T. Yamada, A. Prügel-Bennett, S. Williams, O. Pizarro, and B. Thornton, "GeoCLR: Georeference contrastive learning for efficient seafloor image interpretation," *Field Robotics*, vol. 2, pp. 1134–1155, Mar. 2022. [Online]. Available: https://fieldrobotics.net/Field_Robotics/Volume_2_files/Vol2_37.pdf

[15] T. Yamada, M. Massot-Campos, A. Prügel-Bennett, O. Pizarro, S. B. Williams, and B. Thornton, "Guiding labelling effort for efficient learning with georeferenced images," *IEEE Transactions on Pattern Analysis and Machine Intelligence*, vol. 45, no. 1, pp. 593–607, 2023.